NeuroImage **14,** 347–356 (2001)
doi:10.1006/nimg.2001.0804, available online at http://www.idealibrary.com on IDEAL®

On Multivariate Spectral Analysis of fMRI Time Series

Karsten Müller, Gabriele Lohmann, Volker Bosch, and D. Yves von Cramon

Max-Planck-Institute of Cognitive Neuroscience, P.O. Box 500 355, 04303 Leipzig, Germany

Received September 1, 2000; published online May 30, 2001

Most of functional magnetic resonance imaging (fMRI) time series analysis is based on single voxel data evaluation using parametric statistical tests. The result of such an analysis is a statistical parametric map. Voxels with a high significance value in the parametric test are interpreted as activation regions stimulated by the experimental task. However, for the investigation of functional connectivities it would be interesting to get some detailed information about the temporal dynamics of the blood oxygen level-dependent (BOLD) signal. For investigating that behavior, a method for fMRI data analysis has been developed that is based on Wiener theory of spectral analysis for multivariate time series. Spectral parameters such as coherence measure and phase lead can be estimated. The resulting maps give detailed information on brain regions that belong to a network structure and also show the temporal behavior of the BOLD response function. This paper describes the method and presents a visual fMRI experiment as an example to demonstrate the results. © 2001 Academic Press

Key Words: **fMRI; functional connectivities; spectral analysis; coherence; phase lead.**

INTRODUCTION

The aim of this paper is to show results of investigations on functional connectivities and their temporal dynamics in human brain. With methods of functional magnetic resonance imaging (fMRI), functional network structures can be revealed by investigating the behavior of the blood oxygen level-dependent (BOLD) response function.

There are several approaches that deal with functional connectivities in human brain. Büchel and Friston (1997) used structural equation models. In their treatment, parameters were estimated by minimizing the difference between the observed covariances and those implied by a given structural path or model. The concept of functional and effective connectivities was defined to distinguish statements about observed correlations from results about the influence that one neural system exerts over another (see Friston *et al.*, 1993, 1995c). The structural equation model revealed marked changes in effective connectivity in the posterior visual pathway in relation to the attentional set. Frank *et al.* (1998) developed a probabilistic model allowing the incorporation of relevant prior information and the comparison of data. They defined quantitative measures of activation changes, and they described the level of activation in a voxel compared with the level in another voxel. As a reference voxel, they chose the voxel showing the highest correlation with the model function. Starting from the reference voxel, they localized brain regions that show a high probability of difference.

Recent studies for functional connectivities in human brain deal with the temporal dynamic behavior of the hemodynamic response function across regions in the same subject. Miezin *et al.* (2000) discussed absolute measurements of the variance of the hemodynamic response for one subject, and they determined a rough relation to the likely ordering of activity within the regions. Miezin *et al.* considered the left and right visual and motor cortex and obtained differences for the onset of the response of more than 1 s. They argued that underlying differences in vasculature could make it impossible to reveal interpretable relations. Rosen *et al.* (1998) and Buckner *et al.* (1998a, 1998b) characterized the degree of variability observed in the hemodynamic responses of individual subjects. Different brain regions with an early, mid, and late response were separated. Aguirre *et al.* (1998) also considered the BOLD response within a subject and they concluded that the stability of the response suggests the feasibility of detecting small neuronal onset asynchronies.

Functional connectivities can be described using the correlation structure of the time series either in the time domain or the spectral domain (see Bullmore *et al.*, 1996, Friston *et al.*, 1994b, Worsley and Friston, 1995a, and Zarahn *et al.*, 1997). Most time domain approaches attempt to prewhiten the time series using estimates of the correlation structure, thus enabling an analysis to proceed under the assumption of independence. Prewhitening can be achieved by switching to the spectral domain and using an appropriate spectral density estimate. Marchini and Ripley (2000) adopted this idea and made a new statistical approach to detect

1053-8119/01 $35.00

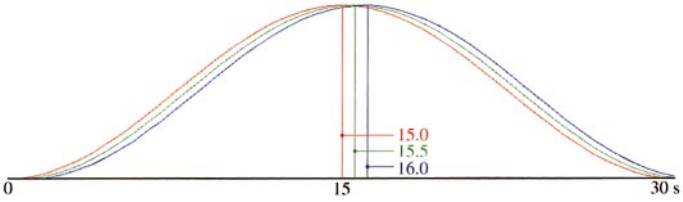

FIG. 1. For validation of the implemented algorithm, a synthetic data set was generated using 10 cycles of a sine function with a full period of 30 s and a time lead up to 1000 ms.

significant activations for experimental designs with periodic stimuli. They introduced a technique to detect periodic activations analyzing the linear model entirely in the frequency domain. Their technique is especially resistant to high frequency artefacts, whereas time domain approaches may be sufficiently susceptible to these effects.

Our approach for evaluation of fMRI data is based on the spectral theory for multivariate time series. As presented in the paper of Marchini and Ripley (2000), we also use a periodic stimulus design and perform the analysis in the spectral domain. Spectral parameters, computed by the spectral density matrix at the fundamental frequency, yield results about functional and effective connectivities in various brain regions. Moreover, these parameters provide detailed information about the temporal dynamics of the BOLD signal in the human brain.

The roots of the described method go back to the findings of Wiener (1949) and Kolmogorov (1941) on prediction theory for weakly stationary stochastic processes. An indexed family of random variables defined in a probability space is called a stochastic process. The concept of stationarity means that the statistical behavior of the stochastic process does not change over time. A stochastic process is called weakly stationary if the mean values are constant in time and the covariances depend only upon the time displacement. Stationary processes arise from any stable system with a steady state mode of operation. Almost all results of spectral theory deal only with such processes and fMRI time series can be considered as weakly stationary. The basic concept and important results of spectral analysis of weakly stationary random processes are outlined in the following section that gives an introduction into mathematical background of the theory. For a detailed treatment, see the books by Hannan (1970) or Brillinger (1975).

The estimation of spectral parameters, such as the sample coherence and the phase lead, is a central issue for investigating fMRI time series. The concept of coherence of time series was introduced by Wiener (1949). It is a measure of the degree of linear association between two time series. Roughly speaking, we may refer to the coherence as a correlation coefficient in the frequency domain. The squared coefficient of coherence can be interpreted as the proportion of the power in one of the two time series (at a selected frequency), which can be explained by its linear regression to the other time course. In fMRI data evaluation, we will compute pairwise coherence coefficients for certain frequencies, which are suggested by the experimental design. Using a fixed threshold, a set of voxels (represented by their fMRI time series) is obtained that form a cluster of voxels with a high coherence coefficient.

For those clusters of voxels with a high sample coherence, the pairwise average phase lead is computed at frequencies suggested by the experimental task. Dividing the phase lead by the frequency, the parameter of time lead of the harmonic of the selected time series can be obtained. Because this is exactly the time lead of the measured signal at two selected voxels, this parameter can be considered as the temporal displacement of the BOLD response in a brain region with respect to another region. For our interpretation, we have to pay attention to the confidence intervals to evaluate the goodness of the estimation. By calculating the time lead for all voxels of the cluster, we will obtain a map of the temporal dynamics of the hemodynamic response.

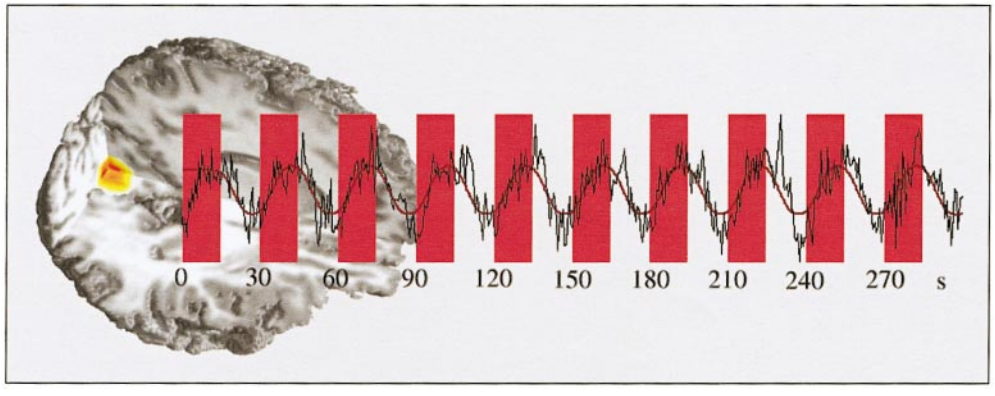

FIG. 2. Fitted response and time course for the most activated voxel. The right visual field was stimulated every 30 s for a duration of 15 s.

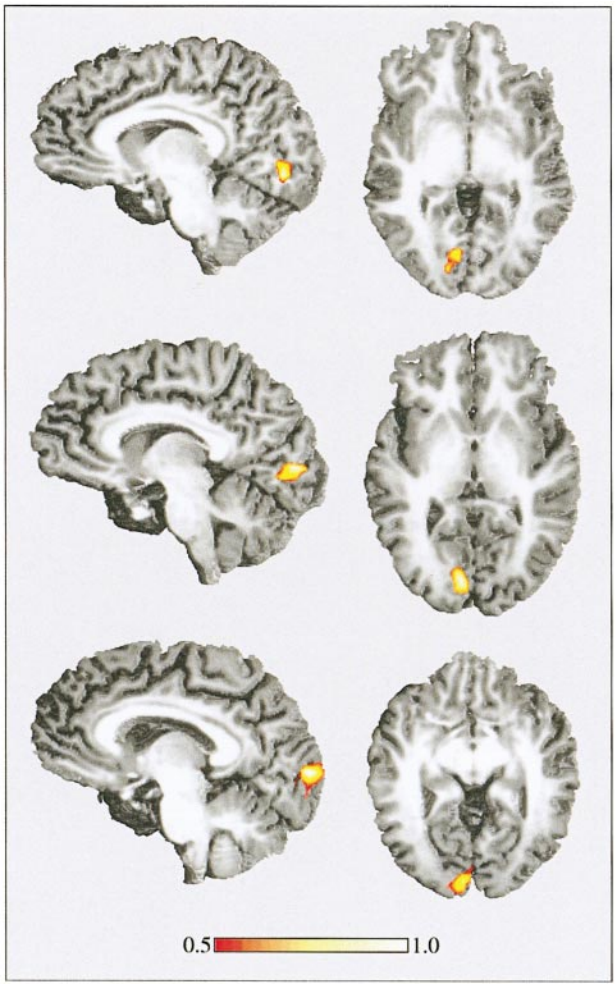

FIG. 3. For each voxel k of the image and a given threshold ρ_0, the number $n_k(\rho_0)$ of voxels with a coherence of more than ρ_0 was computed. The value $n_k(\rho_0)$ is called the number of coherent voxels (ncv) associated with voxel k. For visualization, the maps of ncv were normalized and thresholded, i.e., the maximum was set to 1 and values less than the half of the maximum were set to zero. The maxima of the ncv of all subjects lie around the sulcus calcarine and in adjacent extrastriate visual areas.

To give a demonstration of these results, we will present data from a visual fMRI experiment as an example.

ON SPECTRAL ANALYSIS OF MULTIVARIATE TIME SERIES

In this section, we will give an introduction to the mathematical background of the methods used to investigate the functional connectivities in human brain. The theoretical framework is based on the spectral theory of multivariate time series and, therefore, it is sometimes also called Wiener theory.

Let $\mathbf{X}(t)$ be a vector of time series. In the application of the theory,

$$\mathbf{X}(t) = \begin{pmatrix} X_1(1) \\ \vdots \\ X_n(t) \end{pmatrix}$$

is a vector of fMRI time courses for n voxels, i.e., $X_j(t)$ is the fMRI time course of the voxel j. If this vector contains stochastic processes in the same probability space, $\mathbf{X}(t)$ is called a *multivariate weakly stationary stochastic process* if the mean values are constant in time and the covariances depend upon the time displacement, but not on the time point itself. If $E[X]$ denotes the expectancy value of a random variable X, then $\mathbf{X}(t)$ is a multivariate weakly stationary stochastic process if the following equations hold:

$$E[X_j(t)] = m_j \tag{1}$$

and

$$E[X_j(\tau + t)X_k(t)] = E[X_j(\tau)X_k(0)] = C_{jk}(\tau), \tag{2}$$

where X_j and X_k are arbitrary elements of the vector $\mathbf{X}$. In the case of stationarity, the matrix valued function

$$\mathbf{C}(\tau) = [C_{jk}(\tau)] \tag{3}$$

exists and is called the *cross-covariance function* of the multivariate stationary stochastic process $\mathbf{X}(t)$. For these kinds of time series, there exists the well-known spectral representation

$$C_{jk}(\tau) = \int e^{i\lambda\tau} dF_{jk}(\lambda) \tag{4}$$

with a unique nonnegative Hermitian measure

$$\mathbf{F}(A) = [F_{jk}(A)] \tag{5}$$

and the linear normalized Lebesgue–Borel measure λ on the unit circle. This measure λ can be respected as the angular frequency measured in radians per unit time. Hereafter, without fear of confusion, we will drop the term “angular” and call λ, simply, frequency. The measure $\mathbf{F}$ in equation (4) is called the *cross-spectral distribution* of the stationary stochastic process $\mathbf{X}(t)$ (see, e.g., Koopmans, 1974). Note that the cross-spectral distribution is generally complex-valued because the cross-covariance is not an even function. The elements of the nonnegative Hermitian matrix $\mathbf{F}$ are measures of the relationships between pairs of time series

which belong to the multidimensional stochastic process. The derivative of this function **F** is called the *cross-spectral density function*

$$f_{jk}(\lambda) = \frac{dF_{jk}(\lambda)}{d\lambda} \tag{6}$$

that is the basic parameter for our further considerations. This function can be interpreted as a measure of covariance between the respective frequency components in the two series. The spectral function and the spectral density fulfill the following inequality:

$$|f_{jk}(\lambda)| \leq (f_{jj}(\lambda)f_{kk}(\lambda))^{1/2}. \tag{7}$$

Using the spectral representation in (4), the cross-covariance function can be calculated using the spectral density function represented by

$$C_{jk}(\tau) = \int e^{i\lambda\tau} f_{jk}(\lambda)\, d\lambda. \tag{8}$$

In the following, we will be interested in the relation between two components $X_j(t)$ and $X_k(t)$ of the multivariate stochastic process. The interrelation can be described via the bivariate spectral densities. These parameters are also called bivariate spectral parameters. The polar representation of the spectral density function further gives a set of bivariate spectral parameters which will play a central role in this paper. From the theory of complex numbers, we can write

$$f_{jk}(\lambda) = |f_{jk}(\lambda)| e^{i\vartheta_{jk}(\lambda)}. \tag{9}$$

The function $\vartheta_{jk}(\lambda)$ is called the *phase lead of* $X_j(t)$ *over* $X_k(t)$ and is commonly interpreted as the average phase lag of two time series at frequency λ. This leads to the parameter

$$t_{jk}(\lambda) = \vartheta_{jk}(\lambda)/\lambda, \tag{10}$$

which is the time lead of the harmonic of $X_j(t)$ over $X_k(t)$ at frequency λ. Thus the time lead between two time series can be computed at various frequencies of interest. The coefficient

$$\rho_{jk}(\lambda) = \frac{|f_{jk}(\lambda)|}{(f_{jj}(\lambda)f_{kk}(\lambda))^{1/2}} \tag{11}$$

is called *coherence* and is a crucial parameter for measuring relationships of time series. Using relation (7), the inequality

$$0 \leq \rho_{jk}(\lambda) \leq 1 \tag{12}$$

is satisfied for all frequencies λ. The coefficient of coherence is a measure for the degree of linear association between two time series and can be interpreted quantitatively. The parameter $1 - \rho_{jk}(\lambda)$ is sometimes called the coefficient of incoherence between the time courses $X_j(t)$ and $X_k(t)$ at frequency λ.

A short introduction into the theory of the estimation of spectral parameters is given in the appendix.

Stimuli and Imaging Procedure

A total of 11 subjects (6 female) with a mean age of 25 years participated in the experiment. All were right handed and had normal or corrected-to-normal vision. All subjects provided informed consent prior to the scanning session. Stimuli were projected by an LCD projector onto a back-projection screen mounted in the bore of the magnet behind the subject's head. Subjects viewed the screen wearing mirror glasses, which were equipped with corrective lenses if necessary.

Stimuli consisted of a matrix containing 7 × 12 red L-shaped angles on black background. The matrix was either presented in the left or the right half of the screen with the inner boundary 0.5° from the vertical midline of the screen. The entire matrix had a width of 8.4° and height of 12.3°, where each L had the extension 1° × 0.8°. Every 100 ms, each L was rotated randomly by multiples of 60° so that six orientations were possible. Additionally, a gray fixation cross was presented in the center of the screen. On average, every fourth second the cross disappeared for 200 ms and the subject had to respond via button press. This task was designed to keep the subject alert and to ensure that central fixation was maintained.

Stimulation started with a black screen for 30 s (containing the fixation cross), followed by successive three minute periods of left, no, and right field stimulation. After another 30 s of black screen, the left visual field was stimulated every 30 s for a duration of 15 s; this cycle was repeated 10 times. Following another 30 s of black screen, a similar sequence was presented in the right visual field. Finally, 30 s of black screen were presented.

For our analyses, the initial ten minutes were of no interest. Furthermore, we randomly chose the ten cycles of right visual field stimulation rather than left visual stimulation (see Fig. 2). This was done to restrict the amount of data processing.

Imaging was performed at 3T on a Bruker Medspec 30/100 system and the standard "bird cage" head coil was used. Subjects were laid on the scanner bed and cushions were used to reduce head motion. In addition to the functional data sets high resolution whole brain images were recorded to improve the localization of activation foci using a T1 weighted 3-D segmented

MDEFT sequence (128 slices sagittal, 1.5-mm thickness, 256 × 256 pixel matrix). To align the echo planar images (EPI) to the 3-D images, conventional anatomical images in plane with the functional images were acquired as an intermediate step using a IR-RARE sequence (TE = 20 ms, TR = 3750 ms, 256 × 256 matrix). Finally, functional images were acquired using a gradient EPI sequence (TE = 40 ms, TR = 625, 64 × 64 pixel matrix, 5-mm slice thickness, 2-mm interslice distance, 224-mm FoV), sensitive to BOLD contrast. Data were recorded from five oblique slices with the middle slice containing both the lateral geniculate nuclei and the occipital polar cap.

Validation and Data Analysis

To validate the implemented algorithms, a synthetic data set was generated. The synthetic data set was created with 10 different groups of time courses, generated by a sine function with a full period of 30 s. Between the groups of the synthetic time series, a time lead was chosen from 125 up to 1000 milliseconds (see Fig. 1). The full length of the time series was 300 s. The synthetic data set was generated to be closely aligned to the real data, i.e., the most interesting frequency of 1/30 Hz, as well as the length of the time series is the same as in the experimental data.

The synthetic data set was processed by spectral analysis tools that were implemented as explained in the appendix. As expected, all synthetic blobs have a sample coherence of more than 0.9995. The map of ncv shows the expected pattern, and the value of each voxel coincides exactly with the number of coherent voxels. The values of the generated blobs in the map of phase lead have values that correspond exactly to the time displacement of 125 up to 1000 ms in the synthetic data set.

The fMRI data were processed on a SGI Origin 2000 using software developed at the Max Planck Institute of Cognitive Neuroscience in Leipzig (Germany). Preprocessing, statistics, registration, normalization, and visualization of the data were performed using the software package Lipsia (Lohmann *et al.,* 2000). As already mentioned, the tools for spectral analysis were implemented as explained in the appendix.

The first step of preprocessing contained a slicetime correction using sinc-interpolation. The mathematical basis is the well-known Nyquist–Shannon sampling theorem. Any continuous band-limited function is completely determined by discrete measurements taken at a constant sampling interval. In other words, any function value for which no direct measurement exists can be reconstructed exactly and without loss of information by interpolating between the measurement points (see Press *et al.,* 1992, and James, 1999). The data were also corrected for movement artifacts using a rigid-body realignment. To find the best match for the realignment, we used an optimization algorithm due to Powell (Press *et al.,* 1992). Temporal filtering was done applying a high pass filter for the whole run with a cutoff frequency of 60 s. Filtering was performed by multiplying the signal after Fourier transformation by a sigmoidal cutoff-function and converting it back by the inverse Fourier transform. The effect of such a transformation is a baseline correction of the signal. Preprocessing was finalized by applying spatial filtering using a Gaussian kernel with a standard deviation in pixels of 0.8.

The statistical evaluation was based on a least squares estimation using the general linear model (Winer *et al.,* 1991) for serially autocorrelated observations (see, e.g., Friston, 1994b, and Friston *et al.,* 1995b). The design matrix was generated using a boxcar (square wave) function and a response delay of 6 s. The model includes an empirical estimate of temporal autocorrelation that also reduces the degrees of freedom (Worsley and Friston, 1995). The resulting statistical parametric maps were thresholded at a z value of 3.09 corresponding to a probability of 0.001.

The most computationally expensive part of data processing was the estimation of the spectral density matrix. Each row of this matrix contains the bivariate spectral density of a voxel with all other voxels of the image. The matrix was computed by estimating the multidimensional weighted covariance sequence as described in the appendix. Because the right-field-simulation stimuli were presented every 30 s (for a period of 15 s), the spectral parameters were computed for the frequency of 1/30 Hz. A spectral window size of 60 s was chosen. The equivalent degrees of freedom of the spectral estimator was 26.7.

Using the spectral density matrix, the sample coherence matrix and the matrix of the phase lead estimation were computed (see Eqs. (18) and (19)). These matrices contain the bivariate sample coherence measure and the phase lead estimation of the time courses of all combinations of two voxels of the image. For each voxel k of the image and a given threshold ρ_0, the number $n_k(\rho_0)$ of voxels with a coherence of more than ρ_0 was computed. The value $n_k(\rho_0)$ is called the *number of coherent voxels (ncv) associated with voxel k*. In our data analysis, the value ρ_0 was set to 0.99. We also computed maps of ncv for lower ρ_0. As expected, the values of ncv increased. The shape of the map and the location of the maxima were similar. For each subject, a map of ncv was generated. For visualization, the maps of ncv were normalized and thresholded, i.e., the maximum was set to 1 and values less than half of the maximum were set to zero.

The maxima of the clusters of the maps of ncv were used as starting points for further computations. A map of coherence values was generated by taking the coefficients from the coherence matrix computed before. In practice, that means to take the row of the

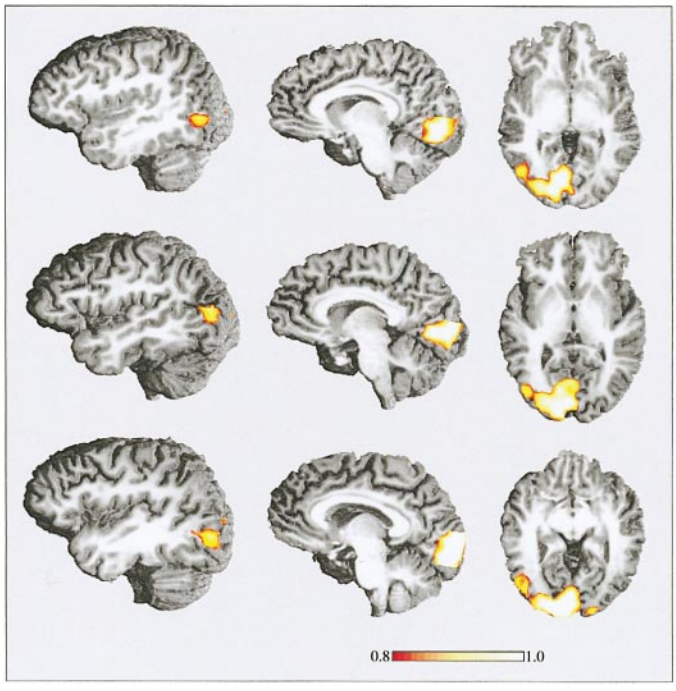

FIG. 4. Maps of sample coherence show visual cortical areas V1/V2 and a region in the vicinity of the lateral occipital sulcus covering O2. The associated maps of confidence intervals show values less than 0.02.

coherence matrix that is associated to the maximum of the map of ncv. These entries were placed onto a map which was overlayed over an anatomical data set. The map of coherence was thresholded, and voxels with a coherence value of more than 0.8 were used to estimate the phase lead as explained in (19).

To evaluate the goodness of the estimation of coherence and phase lead, confidence intervals were computed as described in (21) and (22). Also, maps of confidence intervals were generated for voxels with a coherence value of more than 0.8, and, for visualization, these maps were also overlayed on an anatomical image.

For anatomical localization, the resulting maps of ncv, coherence and phase lead were coregistered onto a 3-D high-resolution T1-weighted anatomical data set using 2-D structural slices that were acquired using MDEFT and EPI-T1 pulse sequences. Although structural EPI-T1 images show less anatomical detail, they are geometrically closer to the functional EPI data than the 2-D MDEFT slices. The algorithm is based on Powell's direction set method in multi dimensions. For a detailed description of coregistration, see Lohmann *et al.* (2000).

RESULTS

The fMRI data were processed as described in the previous section for each subject separately. The resulting maps of ncv have their maximum around the sulcus calcarine and in adjacent extrastriate visual areas (Fig. 3). The maxima of the maps of ncv, i.e., voxels with the largest coherence region, can be considered as centers of activations. The fMRI time series of these voxels have a maximal degree of linear association with the time series of the other voxels (11). The maxima were used to compute estimations for the bivariate coherence and phase lead.

The maps of the sample coherence and the statistical parametric maps show similar patterns for all subjects (see Figs. 4 and 5). Primary visual areas around the sulcus calcarine (areas V1/V2 up to dorsal and lateral regions of V2) revealed a high coherence coefficient as well as a high z score. The occipital polar cap appeared spared. Most likely, because the central visual field was not stimulated. For nine subjects, a region in the vicinity of the lateral occipital sulcus (Duvernoy, 1991) showed a sample coherence above the threshold of 0.8. This area corresponds with the motion area V5. Because the coherence coefficient can be interpreted as the measure of the degree of linear association of time series, the map of coherence shows brain regions that belong to a network structure. In our experiment with visually presented moving L-shaped stimulus, visual cortical areas V1/V2 and V5 belong to that network.

The phase lead of the harmonic of two time series can be considered as the delay of the BOLD response function in a certain brain region with respect to an-

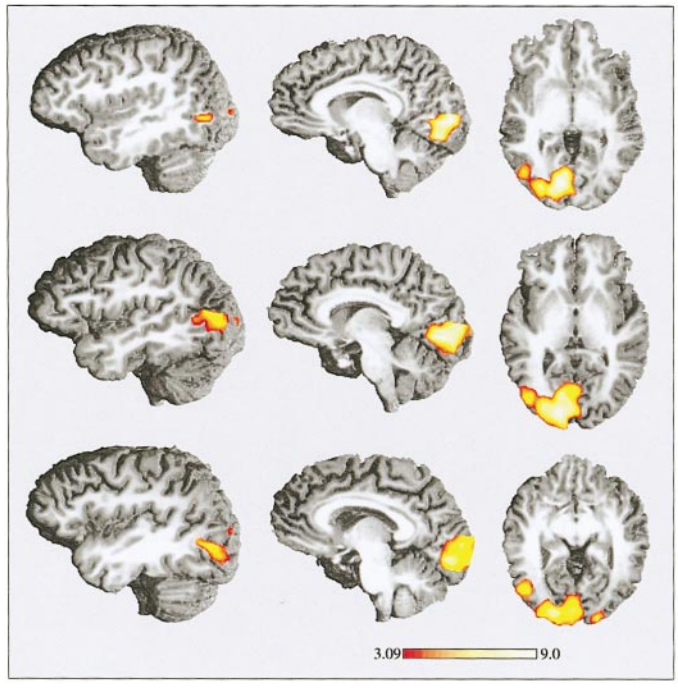

FIG. 5. Statistical parametric maps of z scores obtained by a least squares estimation using the general linear model for serially autocorrelated observations. The pattern of these maps is similar to the maps of sample coherence.

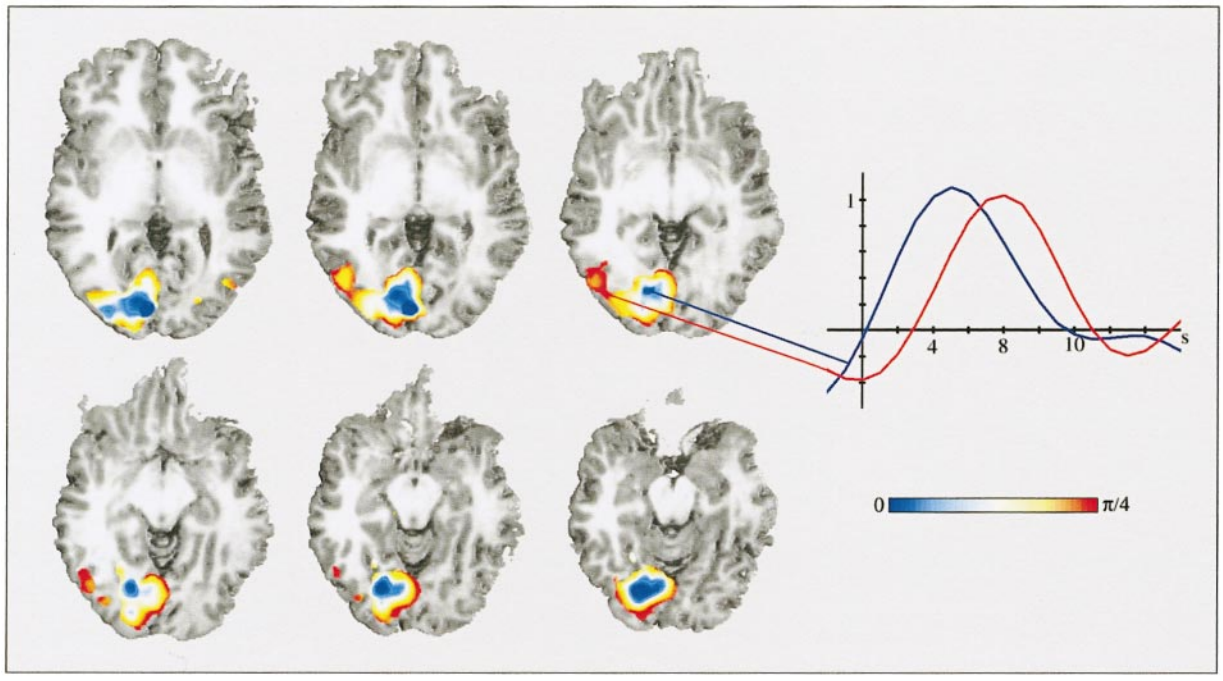

FIG. 6. The phase lead can be interpreted as the time displacement of the hemodynamic response function. This temporal shift is already to be seen in the trial average.

other region. Therefore, the map of phase lead allows conclusions about the temporal behavior of the hemodynamic response function. With the map of phase lead, phase displacements of the BOLD response function are displayed for a given frequency. Brain regions with an early maximum of the response can be separated from those areas with a late BOLD response. The observed phase shifts were unexpected and, therefore, in order to exclude methodological errors, the algorithm was validated by evaluating synthetic data with various phase shifted time series (see previous section for details). The map of phase lead shows exactly the displacements that were implemented in the synthetic data. Furthermore, we also compared the resulting phase maps with the trial averages of the raw data (Fig. 6) that prove that such phase displacements occur indeed.

DISCUSSION

The statistical analysis of fMRI data is often based on the estimation of parameters of a general linear model generated by the design of the experiment (see, e.g., Friston *et al.*, 1994a, 1994b, 1995a, 1995b). Using linear contrasts or compounds, statistical parametric maps can be computed showing which voxels are correlated with the task of the experiment. The resulting statistical parametric map states whether a region is significantly activated or not. For many kinds of brain studies it would be additionally interesting to get more detailed information about functional connectivities and the temporal behavior of the hemodynamic response.

The method described in this paper gives statements on the temporal dynamics of propagation of the BOLD response function. It is based on the spectral theory for weakly stationary stochastic processes. FMRI time series can be considered to be weakly stationary, if we assume that the mean value is constant in time and the covariances depend only on the time displacement and not on the time point itself. This can be assumed for any stable systems with a steady state mode of operation, e.g., for fMRI time series obtained with an experiment with periodic stimulation. However, fMRI time series obtained with stochastic designs can also be assumed to be weakly stationary if the probability of the occurrence of an event does not change over time (see Friston *et al.*, 1999). For the evoked response function, the assumption of weak stationarity (the mean value is constant in time) could be violated by low frequency artefacts due to physiological and technical reasons. However, those trends can be removed applying a temporal high pass filter.

Because of a supposed weakly stationary process, our approach is in particular suitable for analyzing experiments with periodic stimuli. The experimental paradigm is characterized by the fundamental frequency. The core of the method is the estimation of the cross-covariance function and the spectral density matrix. This matrix contains bivariate spectral measures for all combinations of two voxels of the whole brain. The entries of the matrix can be used for computing

estimations of coherence and phase lead. Note that all spectral parameters are functions of the frequency (see Eqs. (15), (18), and (19)). The sample coherence measure can be interpreted as the measure of the degree of linear association of time series. Therefore, brain regions with a high coherence value can be considered as areas that belong to the same network structure. Maps of coherence can be generated for any interesting frequency, e.g., for investigating basic vibrations in human brain. The nature of periodic designs ensures that the components of the spectral measures attributable to the response to the stimulus will occur at a few discrete frequencies in the spectral domain. Because of our experimental design, the spectral parameters at the fundamental frequency contain the majority of information regarding the response to the stimulus. Therefore, at the very last, we estimate the sample coherence and the phase lead at this frequency.

The map of phase lead shows phase displacements of the BOLD response function, and it is used for describing the temporal behavior of the BOLD signal in those brain regions. Because of the preserved relative timing between the onset of the BOLD response in different brain regions, phase displacements can be considered for investigation the temporal behavior of the hemodynamic response. Menon *et al.* (1998) showed that fMRI onset latencies correlate well with independently measurable parameters of the tasks and can be used to determine the origin of processing delays during cognitive and perceptual tasks with a temporal accuracy of tens of milliseconds. They conclude that there are many characteristic features of the fMRI response that can be used to determine latencies between brain areas, and they emphasize the important role for fMRI to study the origin of processing delays in mental operations. We believe that the phase lead, as computed from the spectral density function of the BOLD signal, is one of the characteristic features for detecting relative delays of the response in different brain regions.

Earlier work on single-trial designs (see, e.g., Buckner *et al.*, 1996) demonstrate the possibility to map brain activity by using paradigms similar to those used in evoked potential research that allows to measure timing difference between activation of neuronal substrates in the brain. Rosen *et al.* (1998) and Buckner *et al.* (1998b) also observed additionally time courses of the BOLD response function. They suggested that the robust hemodynamic alterations are detectable after neuronal stimuli lasting only a few tens of milliseconds, and they were able to separate brain regions with an early and late response. Compared with our data, recent work of Miezin *et al.* (2000) showed such displacements of the BOLD response function in the same order of magnitude. Rajapakse *et al.* (1998) extended multiple regression analysis to facilitate the investigation of the variability of hemodynamic parameters of human brain activation. The hemodynamic parameters were estimated across different brain regions and showed significant differences. Kruggel and von Cramon (1999) presented maps of time lags of the hemodynamic response for significantly activated regions from a language processing experiment. In accordance with the results of Rosen *et al.* (1998) and Buckner *et al.* (1998a, 1998b) they were able to differentiate between lag values for early, middle and late responses.

All those approaches are treated in the time domain. In contrast, our results of the evaluation of the synthetic data as well as of the visual fMRI experiment show that spectral methods are also appropriate for investigating functional connectivities in the human brain. It is a fruitful approach that describes the temporal behavior of the BOLD response function. It can be used to gain insight into mutual dependences in a network structure.

APPENDIX

In this section, an introduction is given on how to achieve an estimation of spectral parameters. In the case of stationary random processes, the characteristics of the random variables are estimated by averaging over time and not over realizations.

Let $\mathbf{X}(t)$ be a realization of a multidimensional stationary stochastic process. Without loss of generality, let us assume that $\mathbf{X}(t)$ is already zero-mean. Then the function

$$\hat{C}_{N,jk}(s) = \begin{cases} \dfrac{1}{N} \displaystyle\sum_{t=1}^{N-s} X_j(s+t)X_k(t), & s = 0, 1, \ldots, N-1 \\ \hat{C}_{N,kj}(-s), & s = -1, \ldots, -N+1 \end{cases} \tag{13}$$

is called the *multidimensional weighted covariance estimate* based on the realization $\mathbf{X}(t)$. For $|s| \geq N$, the estimation for the cross-covariance is zero. In this paper, details on the precision of the estimation are omitted.

A naive way to estimate the spectral density of a stationary random process would be to compute the Fourier transform of the multidimensional weighted covariance estimate in (13). The matrix-valued function

$$\hat{P}_{N,jk} = \frac{1}{2\pi} \sum_{s=-(N-1)}^{N-1} e^{-i\lambda s} \hat{C}_{N,jk}(s) \tag{14}$$

is the discrete Fourier transform of the covariance estimate and is often called the *periodogram matrix*. Although the covariance estimate converges to the covariance, its discrete Fourier transform (14) does not

converge to the spectral density. Therefore, in general, the periodogram is not an appropriate estimation for the spectral density of stationary random processes (see Hannan, 1970).

The problem is that, in the neighborhood of N, only a small set of observations are used to estimate the covariance function. In the worst case, only one element of the time course is used. Such an estimation is not admissible. Therefore, a number $M_N < N$ is chosen to determine how many elements of the covariance estimation are used to estimate the spectral density. This number M_N is called the *maximal displacement*, and the estimation of f has the form

$$\hat{f}_{N,jk}(\lambda) = \frac{1}{2\pi} \sum_{s=-M_N}^{M_N} e^{-i\lambda s} w\left(\frac{s}{M_N}\right) \hat{C}_{N,jk}(s). \quad (15)$$

The function w is called a *lag window generator*. With weightings of the covariances it is possible to increase the precision of the estimation of the spectral density. The lag window generator w is a real, even and bounded function which is defined on the interval $[-1, 1]$. There are many kinds of such functions. For our calculations, we will use

$$w(x) = \begin{cases} 1 - 6x^2(1 - |x|), & |x| \le \frac{1}{2} \\ 2(1 - |x|)^3, & \frac{1}{2} \le |x| \le 1 \end{cases}, \quad (16)$$

which is the Parzen lag window generator. This function is very convenient for computing the spectral density estimate. See Priestley (1982) for discussion of other lag window generators. The parameter

$$r_N = 2N\left(\sum_{s=-M_N}^{M_N} w\left(\frac{s}{M_N}\right)\right)^{-1} \quad (17)$$

is computed using the lag window generator and the spectral window. It is called the *equivalent degrees of freedom (EDF)* of the spectral estimator.

Using the estimation in (15), one can give an estimation of the coefficient of coherence of two components $X_j(t)$ and $X_k(t)$ of the multidimensional stationary random process. It has the form

$$\hat{\rho}_{N,jk}(\lambda) = \frac{|\hat{f}_{N,jk}(\lambda)|}{(\hat{f}_{N,jj}(\lambda)\hat{f}_{N,kk}(\lambda))^{1/2}} \quad (18)$$

and is called *sample coherence*. The estimator for the phase lead is

$$\hat{\vartheta}_{N,jk}(\lambda) = \tan^{-1}(\mathrm{Im}\ \hat{f}_{N,jk}(\lambda)/\mathrm{Re}\ \hat{f}_{N,jk}(\lambda)). \quad (19)$$

In this paper, we will compute the sample coherence and give an estimation for the phase angle for different fMRI time series. Because we are also interested in the distribution of the estimated parameters, confidence intervals for the obtained estimations in (18) and (19) are computed. For a detailed treatment, see Hannan's (1970) excellent monograph. For a large number of degrees of freedom ($r_N > 20$), the random variable

$$\varphi_{N,jk}(\lambda) = \tanh^{-1}(\hat{\rho}_{N,jk}(\lambda)) \quad (20)$$

is approximately normally distributed (see Enochson and Goodman, 1965). With straightforward calculation and some algebra, we will get the lower and upper border of the confidence interval

$$\tanh\left\{\varphi_{N,jk}(\lambda) \pm \frac{u_{\alpha/2}(r_N - 2)^{1/2} - 1}{r_N - 2}\right\}, \quad (21)$$

where r_N is the equivalent degrees of freedom (17) and $u_{\alpha/2}$ is taken from the standard normal distribution $\mathcal{N}_{0,1}$. The confidence interval borders of the estimated phase angle can be computed using the term

$$\hat{\vartheta}_{N,jk}(\lambda) \pm \left\{\frac{1 - \hat{\rho}_{N,jk}(\lambda)^2}{(r_N - 2)\hat{\rho}_{N,jk}(\lambda)^2}\right\}^{1/2} t_{2r_N-2}\left(\frac{\alpha}{2}\right), \quad (22)$$

where $\lambda \neq 0, \pi$. The value $t_{2r_N-2}(\alpha/2)$ is taken from the Student's t distribution with $2r_N - 2df$. The confidence intervals are used to gain some information on the goodness of the estimation of the spectral parameters.

REFERENCES

Aguirre, G. K., Zarahn, E., and D'Esposito, M. 1998. The variability of human, BOLD hemodynamic responses. *NeuroImage* **8:** 360–369, doi:10.1006/nimg.1998.0369.

Biswal, B., Yetkin, F. Z., Haughton, V. M., and Hyde, J. S. 1995. Functional connectivity in the motor cortex of resting human brain using echo-planar MRI. *Magn. Reson. Med.* **34:** 537–541.

Brillinger, D. R. 1975. *Time Series—Data Analysis and Theory*. Holt, New York.

Büchel, C., and Friston, K. J. 1997. Modulation of connectivity in visual pathways by attention: Cortical interactions evaluated with structural equation modeling and fMRI. *Cerebral Cortex* **7:** 768–778.

Buckner, R. L., Bandettini, P. A., O'Craven, K. M., Savoy, R. L., Petersen, S. E., Raichle, M. E., and Rosen, B. R. 1996. Detection of cortical activation during averaged single trials of a cognitive task using functional magnetic resonance imaging. *Proc. Natl. Acad. Sci. USA* **93:** 14878–14883.

Buckner, R. L., Koutstaal, W., Schacter, D. L., Wagner, A. D., and Rosen, B. R. 1998. Functional-anatomic study of episodic retrieval using fMRI. I. Retrieval effort versus retrieval success. *NeuroImage* **7:** 151–162, doi:10.1006/nimg.1998.0327.

Buckner, R. L., Koutstaal, W., Schacter, D. L., Dale, A. M., Rotte, M., and Rosen, B. R. 1998. Functional-anatomic study of episodic retrieval. II. Selective averaging of event-related fMRI trials to

test the retrieval success hypothesis. *NeuroImage* **7:** 163–175, doi:10.1006/nimg.1998.0328.

Bullmore, E. T., Rabe-Hesketh, S., Morris, R. G., Williams, S. C. R., Gregory, L., Gray, J. A., and Brammer, M. J. 1996. Functional magnetic resonance image analysis of a large-scale neurocognitive network. *NeuroImage* **4:** 16–33, doi:10.1006/nimg.1996.0026.

Duvernoy, H. 1991. *The Human Brain. Surface, Three-Dimensional Sectional Anatomy and MRI.* Springer, Wien.

Enochson, L. D., and Goodman, N. R. 1965. Gaussian approximation to the distribution of sample coherence. Res. and Technol. Div., AFSC, Wright-Patterson AFB, OH. AFFDL TR 65–67.

Frank, L. R., Buxton, R. B., and Wong, E. C. 1998. Probabilistic analysis of functional magnetic resonance imaging data. *Magn. Reson. Med.* **39:** 132–148.

Friston, K. J., Frith, C. D., Liddle, P. F., and Frackowiak, R. S. J. 1993. Functional connectivity: The principal component analysis of large (PET) data sets. *Cereb. Blood Flow Metab.* **13:** 5–14.

Friston, K. J. 1994a. Statistical parametric mapping. In *Functional Neuroimaging* (R. W. Thatcher, M. Hallet, T. Zeffiro, E. R. John, and M. Huerta, Eds.), pp. 79–93. Academic Press, San Diego.

Friston, K. J. 1994b. Statistical parametric maps in functional imaging: A general linear approach. *Hum. Brain Mapp.* **2:** 189–210.

Friston, K. J., Holmes, A. P., Poline, J.-B., Grasby, B. J., Williams, C. R., Frackowiak, R. S. J., and Turner, R. 1995a. Analysis of fMRI time-series revisited. *NeuroImage* **2:** 45–53, doi:10.1006/nimg.1995.1007.

Friston, K. J., Holmes, A. P., Worsley, K. J., Poline, J. P., Frith, C. D., and Frackowiak, R. S. J. 1995b. Statistical parametric maps in functional imaging: A general linear approach. *Hum. Brain Mapp.* **2:** 189–210.

Friston, K. J., Ungerleider, L. G., Jezzard, P., and Turner, R. 1995c. Characterizing modulatory interactions between V1 and V2 in human cortex with fMRI. *Hum. Brain Mapp.* **2:** 211–224.

Friston, K. J., Zarahn, E., Josephs, O., Henson, R. N. A., and Dale, A. M. 1999. Stochastic designs in event-related fMRI. *NeuroImage* **10:** 607–619, doi:10.1006/nimg.1999.0498.

Hannan, E. J. 1970. *Multiple Time Series.* Wiley, New York.

James, G. 1999. *Advanced Modern Engineering Mathematics.* Addison Wesley, Harlow, England.

Kolmogorov, A. N. 1941. Stationary sequences in Hilbert space. *Bull. Math. Univ. Moscow* **2**(6): 40 pp. [Russian; English translation by Natasha Artin.]

Koopmans, L. H. 1974. The Spectral Analysis of Time Series. In *Probability and Mathematical Statistics* (Z. W. Birnbaum and E. Lukacs, Eds.), Vol. 22. Academic Press, New York/San Francisco/London.

Kruggel, F., and von Cramon, D. Y. 1999. Temporal properties of the hemodynamic response in functional MRI. *Hum. Brain Mapp.* **8:** 259–271.

Lohmann, G., Müller, K., Bosch, V., Hessler, S., Mentzel, H., and von Cramon, D. Y. 2000. Lipsia—A software package for evaluation of functional mri data. Technical report, Max-Planck Institute of Cognitive Neuroscience, Leipzig, Germany, www.cns.mpg.de/lipsia.

Lohmann, G., Müller, K., Bosch, V., Mentzel, H., Hessler, S., Chen, L., and von Cramon, D. Y. 2001. Lipsia—A new software system for the evaluation of functional magnetic resonance images of the human brain. *Comput. Med. Imaging Graph.,* in press.

Lowe, M. J., Mock, B. J., and Sorenson, J. A. 1998. Functional connectivity in single and multislice echoplanar imaging using resting-state fluctuations. *NeuroImage* **7:** 119–132, doi:10.1006/nimg.1997.0315.

Marchini, J. L., and Ripley, B. D. 2000. A new statistical approach to detecting significant activation in functional MRI. *NeuroImage* **12:** 366–380, doi:10.1006/nimg.2000.0628.

Menon, R. S., Luknowsky, D. C., and Gati, J. S. 1998. Mental chronometry using latency-resolved functional MRI. *Proc. Natl. Acad. Sci. USA* **95:** 10902–10907.

Miezin, F. M., Maccotta, L., Ollinger, J. M., Petersen, S. E., and Buckner, R. L. 2000. Characterizing the hemodynamic response: Effects of presentation rate, sampling procedure, and the possibility of ordering brain activity based on relative timing. *NeuroImage* **11:** 735–759, doi:10.1006/nimg.2000.0568.

Press, W. H., Teukolsky, S. A., Vetterling, W. T., and Flannery, B. P. 1992. *Numerical Recipes in C.* Cambridge Univ. Press.

Priestley, M. B. 1981. Spectral Analysis and Time Series. In *Probability and Mathematical Statistics.* Academic Press, London.

Rajapakse, J. C., Kruggel, F., Maisog, J. M., and von Cramon, D. Y. 1998. Modeling hemodynamic response for analysis of functional MRI time-series. *Hum. Brain Mapp.* **6:** 283–300.

Rosen, B. R., Buckner, R. L., and Dale, A. M. 1998. Event-related functional MRI: Past, present, and future. *Proc. Natl. Acad. Sci. USA* **95:** 773–780.

Wiener, N. 1949. *Extrapolation, Interpolation, and Smoothing of Stationary Time Series with Engineering Applications.* MIT Press, Cambridge, MA; Wiley, New York; Chapman & Hall, London.

Winer, B., Brown, D., and Michels, K. 1991. *Statistical Principles in Experimental Design.* McGraw-Hill series in psychology, New York.

Worsley, K. J., and Friston, K. J. 1995. Analysis of fMRI time-series revisited—Again. *NeuroImage* **2:** 359–365, doi:10.1006/nimg.1995.1023.

Zarahn, E., Aguirre, G. K., and D'Esposito, M. 1997. Empirical analyses of BOLD fMRI statistics. *NeuroImage* **5:** 179–197, doi:10.1006/nimg.1997.0263.